Systems/Circuits

Circadian Regulation of the Rod Contribution to Mesopic Vision in Mice

Annette E. Allen
Division of Neuroscience and Experimental Psychology, Faculty of Biology, Medicine, and Health, University of Manchester, Manchester M13 9PT, United Kingdom

At intermediate (mesopic) light levels, rods and cones are both active and can contribute to vision. This presents a challenge to the retina because the visual responses originating with rods and cones are distinct, yet their visual responses must be seamlessly combined. The current study aimed to establish how the circadian clock regulates rod and/or cone vision in these conditions, given the strong time-of-day change in the reliance on each photoreceptor. Visual responses were recorded in the retina and visual thalamus of anaesthetized male mice at distinct circadian time points, and the method of receptor silent substitution was used to selectively stimulate different photoreceptor types. With stimuli designed to only activate rods, responses in the mesopic range were highly rhythmic and peaked in amplitude in the subjective night. This rhythm was abolished following intravitreal injection of the gap junction blocker meclofenamic acid, consistent with a circadian variation in the strength of electrical coupling of photoreceptors. In contrast, responses to stimuli designed to only activate cones were arrhythmic within the mesopic to photopic range when adapted to the background irradiance. The outcome was that combined rod-plus-cone responses showed a stable contrast-response relationship across mesopic-photopic backgrounds in the circadian day, whereas at night, responses were significantly amplified at lower light levels. These data support the idea that the circadian clock is a key regulator of vision, in this case defining the relative amplitude of rod/cone vision across the mesopic transition according to time of day.

Key words: **circadian; cone; electroretinogram; mesopic; photoreceptor; rod**

Significance Statement

Although the importance of circadian clocks in regulating vision has been long recognized, less is known about how the clock shapes vision in conditions where both rods and cones are active (mesopic conditions). Here, the novel approach of receptor silent substitution has been applied to trace rod and cone visual responses in mice across the circadian cycle and has identified pronounced rhythms in rod, but not cone, vision. This has the effect of boosting responses in dimmer backgrounds at night at the cost of impaired contrast–response stability across the mesopic to photopic range. Thus, the circadian clock drives anticipatory changes in the relative contribution of rods versus cones to vision, which match the prevailing visual environment.

Introduction

Rod and cone photoreceptors allow organisms to sense and respond to light across the huge range of illumination that is encountered in the natural world. Although vision is exclusively supported by rods or cones at the extremes of starlight and sunlight, at intermediate (mesopic) light levels, rods and cones are both active and can contribute to vision. The retina is therefore faced with the challenge of combining information from two distinct systems that are operating at opposite extremes of their sensitivity range and that differ in some basic properties, for example, response kinetics, downstream circuitry, and contrast sensitivity (Umino et al., 2008; Naarendorp et al., 2010).

In mesopic conditions, visual signals from rods and cones converge at several points in the retina (Bloomfield and Dacheux, 2001), and changes in the behavior of those circuits can define the extent to which vision originates with either photoreceptor as well as the properties of those visual signals. In many cases, these adjustments follow a change in background light intensity, which drives adaptational changes in individual cells and circuits and can lead to saturation or adaptation of distinct downstream pathways. However, many of these neural mechanisms are also under the control of retinal circadian clocks, which drive rhythms in the release of or

Received Mar. 9, 2022; revised July 27, 2022; accepted Sep. 21, 2022.

Author contributions: A.E.A. designed research; A.E.A. performed research; A.E.A. analyzed data; A.E.A. wrote the paper.

A.E.A. was supported by a Sir Henry Dale Fellowship, jointly funded by Wellcome Trust and Royal Society Grant 218556/Z/19/Z. The author thanks Prof. Rob Lucas, Dr. Bea Bano-Otalora, Dr. Nina Milosavljevic, and Dr. Riccardo Storchi for comments on the manuscript, and Dr. Franck Martial for technical support.

The author declares no competing financial interests.

Correspondence should be addressed to Annette E. Allen at Annette.allen@manchester.ac.uk.

https://doi.org/10.1523/JNEUROSCI.0486-22.2022

sensitivity to retinal neuromodulators (Tosini and Menaker, 1996; Doyle et al., 2002; Fukuhara et al., 2004; Ribelayga and Mangel, 2005), the electrical coupling of rods and cones (Ribelayga et al., 2008), the photoreceptor cAMP signaling cascade (Fukuhara et al., 2004), and disk shedding (LaVail, 1976). Therefore, there is strong evidence that the circadian clock plays an important role in regulating the balance of rod versus cone vision.

Most of our knowledge on how the clock regulates rod/cone function in the mouse comes from the electroretinogram (ERG; Cameron et al., 2008b), focusing on responses at the extremes of visual sensitivity. Cone ERG responses can be isolated in the presence of a bright, rod-saturating, background light (Peachey and Ball, 2003). In these conditions, the cone b-wave amplitude peaks in the subjective daytime in wild-type (Barnard et al., 2006; Storch et al., 2007; Cameron et al., 2008a; Sengupta et al., 2011) and *Gnat1*$^{-/-}$ (rod-less) mice (Cameron and Lucas, 2009), and rhythms are eliminated in mice with lesions in clock genes (Storch et al., 2007; Cameron et al., 2008a; Ait-Hmyed Hakkari et al., 2016; Wong et al., 2018). Conversely, rod responses can be isolated by measuring their amplitude below cone threshold, presenting very dim flashes of light against darkness. Evidence suggests that the clock does not regulate vision in these circumstances (Storch et al., 2007; Cameron et al., 2008a; Sengupta et al., 2011), although rhythms are reported by Gegnaw et al. (2021). The absence of rhythms in the rod ERG is consistent with the finding that absolute threshold responses of retinal ganglion cells are arrhythmic (Koskela et al., 2020).

The question of how the clock shapes rod versus cone vision at intermediate intensities when both are active remains largely unexplored. This is despite the fact that this is perhaps the most physiologically relevant expression of a change in rod/cone contributions to vision. The approach of receptor silent substitution provides a unique opportunity to tackle this deficit. By using carefully calibrated stimulus spectra, the response of different classes of photoreceptors can be measured in isolation but within an intact system (Brown et al., 2012). This means that responses originating with cones can be isolated at light intensities in which rods are still active (i.e., mesopic conditions) and vice versa. Here, this approach has been applied to anesthetized mice to establish for the first time how the relative amplitude of rod- versus cone-driven visual responses changes across the circadian day, at the level of the retina (ERG) and brain (dorsal lateral geniculate nucleus; dLGN), and across the mesopic-to-photopic range.

Materials and Methods

Animals. All experiments were performed in *Opn1mw*^{R} mice (male, age 4–7 months) on a C57/BL6 background (RRID:MGI:2678771). *Opn1mw*^{R} refers to the transgenic allele originally generated by Smallwood et al. (2003), and termed "R" by them. All animal care was in accordance with the Animals, Scientific Procedures, Act of 1986 (United Kingdom) and approved by the local (University of Manchester) ethics committee. Before experiments, all animals were kept in a 12 h light/dark cycle at a temperature of 22°C with food and water available *ad libitum*.

Electroretinography. Anesthesia was induced with an intraperitoneal injection of ketamine (100 mg/kg body weight) and medetomidine (1 mg/kg body weight). A topical mydriatic (tropicamide 1%, Bausch & Lomb) and hypromellose eye drops were applied to the recording eye before placement of a corneal contact lens–type electrode. Mice were placed onto a bite bar for head support, which also acted as a ground. A needle reference electrode (Ambu, Neuroline) was inserted ~5 mm from the base of the contralateral eye. Electrodes were connected to a Windows PC via a signal conditioner (model 1902 Mark III, Cambridge Electronic Design) that differentially amplified (× 3000) and filtered (bandpass filter cutoff, 0.5–200 Hz) the signal and to a digitizer (Model 1401, Cambridge Electronic Design). Core body temperature was maintained at 37°C throughout recording with a homeothermic heat mat (Harvard Apparatus). Following the first ERG recording, anesthesia was reversed by intraperitoneal injection of atipamezole (3 mg/kg body weight).

ERGs were recorded at subjective dawn, [circadian time (CT)0], midday (CT6), dusk (CT12), or midnight (CT18), following dark adaptation for a period of at least 18 h (Fig. 1). Mice were housed for >2 weeks in a 12 h light/dark cycle.

In vivo electrophysiology. All dLGN recordings were performed at subjective midday (CT6), and midnight (CT18) as described above, with experimental setup performed under a dim red light. Anesthesia was induced with an intraperitoneal injection of urethane (1.5 × g/kg 30% w/v; Sigma-Aldrich). A topical mydriatic (1% w/v atropine sulfate; Sigma-Aldrich) and mineral oil (Sigma-Aldrich) were applied to the eye before recordings. After placement into a stereotaxic frame, the skull surface of the mouse was exposed and a hole drilled ~2.3 mm posterior and ~2.2 mm lateral to the bregma. A recording probe (A4x16-Poly2-5 mm-23 s-200-177-A64; NeuroNexus) was lowered to a depth of ~2.5–3 mm into the brain, targeting the dorsal lateral dLGN. Neural signals were acquired using a Recorder64 system (Plexon), and were amplified (× 3000), high-pass filtered (300 Hz), and digitized at 40 kHz. Multiunit activity was saved and analyzed off-line using Offline Sorter (Plexon). After removing artifacts common to all channels, single-unit spikes were detected and categorized based on the spike waveform via a principal component analysis whereby distinct clusters of spikes were readily identifiable, which showed a clear refractory period in their interspike interval distribution. Spike-sorted data were then further analyzed using MATLAB R2018a (MathWorks) to assess the changes in then firing rate of neurons in response to different visual stimuli.

Visual stimuli. Regarding light calibration, stimuli were measured at the corneal plane using a spectroradiometer (Bentham Instruments) between 300 and 700 nM. The effective photon flux for each photopigment was then calculated by weighting spectral irradiance according to pigment spectral efficiency function (derived from a visual pigment template; Govardovskii et al., 2000) and λ max values of 365, 480, 498, and 556 nm for short-wavelength-sensitive (SWS) opsin, melanopsin, rod opsin, and the introduced long-wavelength-sensitive (LWS) opsin, respectively, multiplied by an *in vivo* measurement of spectral lens transmission (Jacobs and Williams, 2007). The approach is equivalent to that described in Lucas et al. (2012).

Visual stimuli were generated with a combination of violet, blue, cyan, yellow, and red elements of a multispectral LED light source (for ERGs, Lumencor; for dLGN recordings, CoolLED). Intensities were modulated via pulse width modulations using an Arduino Uno. Light from the light engine passed through a filter wheel containing neutral-density filters (reducing the light by between 10^1 and 10^5) and focused onto an opal diffusing glass (5 mm diameter; Edmund Optics) positioned <5 mm from the eye. All LED intensities were controlled dynamically with a PC.

LEDs were combined to generate three initial spectra that are summarized in Figure 1. Transitions between stimuli were designed to be apparent for rods and remain isoluminant for LWS and SWS opsins [68% Michelson contrast for rod opsin; intensity of (unattenuated) background spectrum, 15.2 rod effective photons/cm 2/s] or vice versa [64% Michelson contrast for LWS and SWS opsin; intensity of (unattenuated) background spectrum, 15.6 and 14.1 LWS and SWS effective photons/cm 2/s]. Because all photoreceptor-isolating stimuli were designed relative to a common background spectrum, stimuli targeting different classes of photoreceptors were presented in an interleaved design. Unless explicitly specified, all light-adapted stimuli were presented following 10 min adaptation to the background spectrum, with stimuli ordered from dimmest to brightest. Stimuli were presented either as a flash of stimulus spectra from background (50 ms, 950 ms interstimulus interval) or square-wave steps from background to stimulus spectrum (0.5, 4, 8, 16, 25, 33, 40, 50 Hz). The unattenuated background

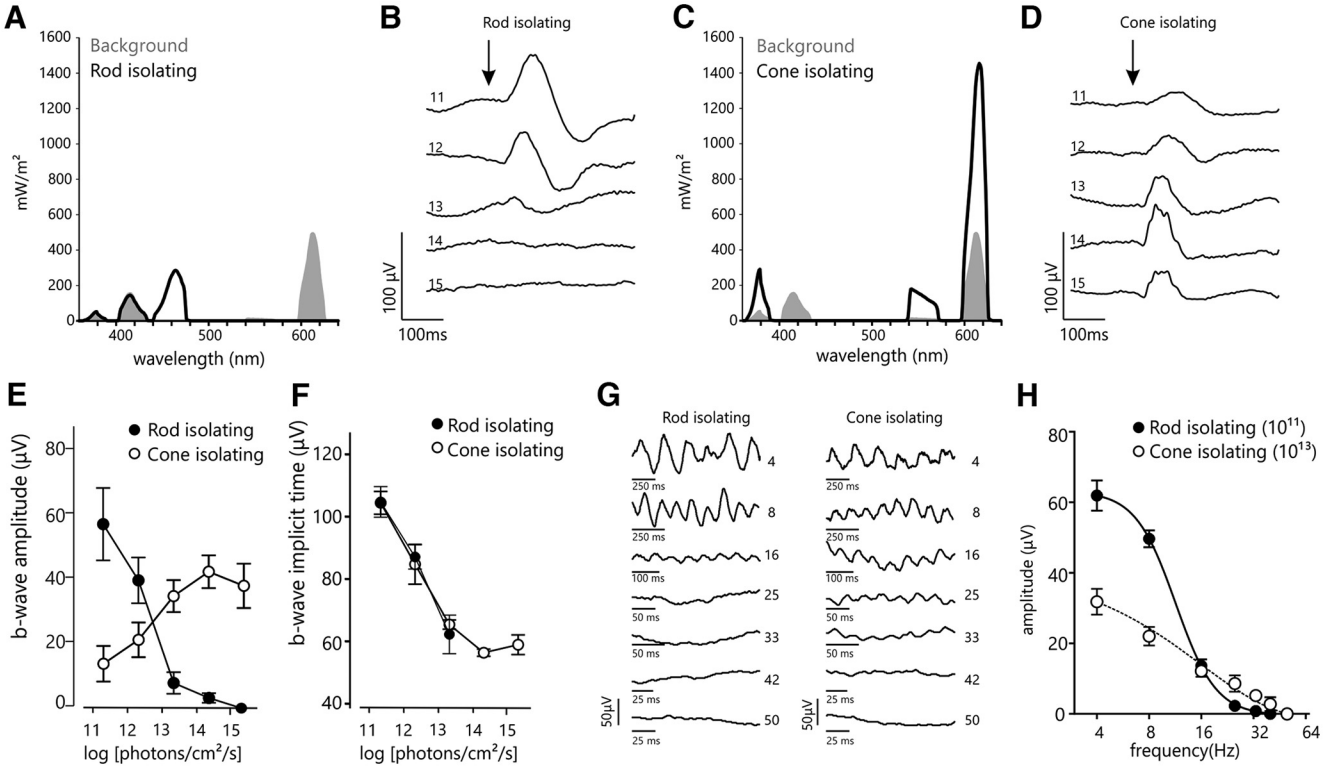

Figure 1. Stimulus spectra used to isolate rod and cone responses. ***A***, The output of a four-primary LED light source was adjusted to generate a pair of spectra that presented contrast for rod opsin and remained isoluminant for short (S) and long (L) wavelength sensitive cone opsins. Gray, background spectrum; black, rod-isolating spectrum. ***B***, Representative ERG responses recorded in response to a transition between rod-isolating spectra at five different mean light levels. Left, Log rod-effective photons/cm^2/s; arrow indicates flash onset. ***C***, Spectra as in ***A*** but designed to present contrast for L and S cone opsins (black. cone-isolating spectrum). ***D***, representative ERG responses recorded in response to a transition between cone-isolating spectra at five different mean light levels. Left, Log cone-effective photons/cm^2/s; arrow indicates flash onset. ***E***, ***F***, b-Wave amplitude (***E***) and implicit time (***F***) measured in response to rod-isolating (black) and cone-isolating (white) stimuli as a function of background light intensity (n = 6/group). Data show mean ± SEM. ***G***, Representative ERG responses in response to rod-isolating (left) and cone-isolating (right) stimuli presented as square wave flickers at frequencies of 4–50 Hz. ***H***, Flicker response amplitude in response to rod and cone-isolating stimuli, as a function of flicker frequency. Data show mean ± SEM.

spectrum had the following alpha-opic lux values: 10,295 erythropic lux, 1702 cyanopic lux, 4981 rhodopic lux, 7307 melanopic lux, and a power of 3.91 µW/cm^2. To establish contrast–response curves, background and stimulus spectra were mixed to varying ratios, according to a gamma-corrected curve for each LED. These stimuli were then validated using a spectroradiometer (either from Bentham Instruments or the SpectroCAL II, Cambridge Research Systems). Two further stimuli were used, which presented contrast to rods and cones in concert. First, a spectrally neutral energy stimulus was presented, which was designed to recreate the high-contrast photopic flash stimulus used previously (Cameron et al., 2008a; ~87% Michelson contrast). A second stimulus (termed "rod-plus-cone") was designed to present the sum of rod-only and cone-only stimuli (i.e., matched contrast for individual stimuli; maximum Michelson contrast ~68%).

Stimulus validation. To experimentally validate rod- and cone-isolating stimuli, ERG responses were recorded to each stimulus over a four-log unit range of light intensities, covering the mesopic to photopic range (11–15 log photons/cm^2/s). In agreement with previously published data using similar approaches (Allen and Lucas, 2016; Tsai et al., 2017), a progressive decrease in b-wave amplitude elicited by the rod stimulus was observed along with a corresponding increase in b-wave amplitude to the cone stimulus as background light intensities increased (Fig. 1). For further validation, we then presented each of these stimuli at a range of flicker frequencies. The flicker fusion frequency was ~16 Hz for the rod-targeting stimulus (measured at 11.1 log photons/cm^2/s) but ~33 Hz with the cone-targeting stimulus (measured at 13.1 log photons/cm^2/s; Fig. 1*G*,*H*).

Intravitreal injections. Intravitreal injections were conducted on anesthetized mice with pupils dilated, as described above. About 2 µl of 1 mM meclofenamic acid (MFA; Sigma-Aldrich) or vehicle control (saline) was injected into the vitreous of the right eye using a Nanofil 10 µl syringe (World Precision Instruments) with a 35 gauge beveled needle. Post-treatment ERG recordings were made 30 min after injection and compared against preinjection responses from the same eye.

ERG analysis. ERG a-waves were not readily measurable using light-adapted stimuli. ERG b-wave amplitude and implicit times were measured relative to baseline values taken at stimulus onset; d-wave amplitudes, where measurable, were measured relative to baseline values taken at light offset. For flicker stimuli, the mean peak to trough response to the first three cycles of each stimulus was calculated.

dLGN analysis. Perievent histograms (bin size 50 ms) were generated for all units in response to rod/cone/rod-plus-cone-isolating stimuli at two irradiances. Units were classed as light responsive if the mean firing rate during the presentation of a stimulus exceeded 2× the SD of the prestimulus firing. For each light responsive unit, the change in response was calculated by comparing the mean firing rate in the 250 ms following the stimulus onset with the 250 ms before stimulus onset. A high-resolution perievent histogram was also generated with a bin size of 10 ms and 50 ms moving average, and the time at which firing activity exceeded 2× the SD of prestimulus firing rate was used to define response latency. Because multiple neurons were recorded in each animal, changes in firing rate were compared using a multilevel mixed-effects linear model that included the animal that each cell was recorded from as a random effect and the time of day as fixed effect.

Experimental design and statistical analysis. For comparisons of ERG b-wave amplitudes or implicit times, two-way repeated measures ANOVAs were used with the nominal factors being irradiance/contrast and circadian time. *Post hoc* Bonferroni tests were performed to test mean values in individual circadian and/or irradiance pairings. All data for rod/cone/energy stimuli were collected in parallel from the same

animals in an interleaved fashion. For comparisons made at only two circadian time points (see Fig. 7), data were collected from the same set of animals on two separate occasions (with the order of conditions randomized). All data were visualized and statistically examined using MATLAB (release 2018a, MathWorks), SPSS version 28, and GraphPad (version 8.4.3) software. For all tests, statistical significance was set at $p < 0.05$. Data are expressed as mean ± SEM. Numbers of mice and p values are indicated in the text or figure legends. Data are available on request.

Results

Mesopic cone vision is not regulated by the circadian clock

The photopic ERG is highly rhythmic, but it is not clear whether this rhythmicity extends to cone vision following adaptation to the background irradiance and/or light intensities in which both rods and cones are active. To address this, the experimental approach of receptor silent substitution was used, which allows cone responses to be recorded in conditions in which rods are also active (Rushton, 1972; Estevez and Spekreijse, 1982). In this approach, variations in the stimulus spectra are used to present contrast for one photoreceptor but present nominal contrast (remain silent) for others. To maximize the capability of this method, *Opn1mw*^{R} mice were used, in which the native mouse medium-wavelength-sensitive (green) cone opsin is replaced by the human LWS (red) opsin (Smallwood et al., 2003), providing a greater separation in the spectral sensitivity of rod opsin and cone opsins. Validation of this approach is shown in Figure 1 and is described in the methods. As expected, our data revealed an irradiance-dependent transition from rod to cone vision and defined the range over which both rod and cone ERGs were measurable in this experimental setting, that is, mesopic vision.

Light-adapted ERGs were recorded in anesthetized mice at four different phases of the circadian day—dawn, midday, dusk, and midnight (CT0, CT6, CT12, and CT18). At each circadian time point, 50 ms flashes of a cone stimulus were presented with a range of contrasts (maximum 64% Michelson contrast), and at four mean background light intensities (11.3–14.3 log cone photons/cm^2/s). Responses were recorded in sequence from the dimmest to brightest background and following 10 min adaptation to each background. Cone ERG b-waves reflecting the activity of ON-bipolar cells (Stockton and Slaughter, 1989) were measurable across this intensity range and showed a gradual increase in amplitude and reduction in implicit time as background irradiance increased (Fig. 2*A–C*). However, at all contrasts/backgrounds tested, there was no significant variation in cone b-wave amplitude or implicit time according to time of day (two-way ANOVA finds a significant effect of irradiance, $p < 0.01$) but not CT or the interaction between CT and irradiance ($p > 0.05$; Fig. 2*B–F*). This was also true using square wave flickers of increasing frequencies in which no measurable difference was detected in the cone-driven response between CT6 and CT18 (Fig. 2*G*,*H*).

Rhythms in photopic ERGs originate with cones

These results contrast with the overt circadian rhythm that is reported in the photopic ERG, recorded immediately after moving from dark-adapted to light-adapted conditions. Such paradigms essentially test the ability of the retina to light adapt, so one explanation is that they reveal a rhythm in the efficiency of cone adaptation. However, it is also formally possible that the failure to detect rhythms in cone responses is because of the limits on stimulus contrast that are achievable with the silent substitution approach. Finally, it remains unknown whether the photopic ERG is exclusively cone driven, given that rod recovery from bleach can occur across longer time frames (Tikidji-Hamburyan et al., 2017).

To differentiate between these possibilities, flashes of a rod-isolating, cone-isolating, and high-contrast energy stimulus (exciting both rods and cones, ~88% Michelson contrast) were presented against a photopic background (15.3 log cone photons/cm^2/s; 50 ms flashes presented every 950 ms in an interleaved pattern) for 20 min, immediately after a transition from dark-adapted to light-adapted conditions. Rod responses were not measurable across the time course, at any CT tested, confirming a minimal contribution of rods to the photopic ERG (Fig. 3*A*). In contrast, ERG b-waves were measurable in response to the energy and cone-isolating stimuli, and both showed increases in b-wave amplitude and reduction in implicit time throughout the course of light adaptation (Fig. 3*D*,*E*,*H*,*I*). However, in both cases, the amplitude and implicit time was dependent on circadian time, with faster and larger responses recorded in the circadian day, peaking at CT6 (Fig. 3*D–K*). Although this effect was most pronounced using the energy stimulus, where amplitudes were larger (consistent with the enhanced contrast of this stimulus), critically, a significant rhythm was also apparent when isolating responses only from cones, confirming rhythmicity in cone vision in these circumstances. The enhanced response amplitude at CT6 versus CT18 was also apparent in response to cone-isolating stimuli presented in mesopic conditions (background, 12.7 log photons/cm^2/s; Fig. 3*L*,*M*). However, response amplitudes were no longer significantly different after 20 min adaptation, consistent with the view that adaptation overcomes initial time-of-day changes in the cone ERG.

The amplitude of mesopic rod responses peaks in the subjective night

The focus was next turned to rod vision. At each of four circadian time points, 50 ms flashes of the rod stimulus (separated by 950 ms background) were presented at a range of contrasts (maximum 68% Michelson contrast) and at four mean background light intensities (11.3–14.3 log rod photons/cm^2/s) and after a period of 10 min adaptation to each background. Rod responses showed a steady decrease in amplitude and a decrease in implicit time as the background irradiance level increased (Fig. 4*A–C*), consistent with previous reports of rod vision (Altimus et al., 2008; Naarendorp et al., 2010; Tikidji-Hamburyan et al., 2017; Umino et al., 2019). However, there was a significant variation in response amplitude measured at different circadian times. Specifically, rod b-waves were larger in the subjective early and midnight (CT12 and CT18) compared with the early and midday (CT0 and CT6) so that irradiance response curves for rod b-wave amplitudes were significantly dampened at CT0 and CT6 (Fig. 4*B–F*). The same was true for contrast–response curves measured at each irradiance (shown for the dimmest background in Fig. 4*D*). The result was that for certain irradiance/contrast pairings, rod ERGs were measurable in the subjective night but not day. The EC_{50} of curves fitted to b-wave amplitude versus irradiance was not significantly different between CTs (only in their maximum amplitude), indicating a change in gain. The same was true for curves fitted to b-wave amplitude versus contrast, suggesting no change in absolute sensitivity. Unlike amplitude, there was no change in the implicit time of rod b-waves as a function of time of day across all conditions tested (profile of maximum intensity at 11.3 log rod photons/cm^2/s shown in Fig. 4*F*). Rhythmicity in the rod ERG was also tracked over the time course of adaptation by presenting rod-isolating stimuli at the

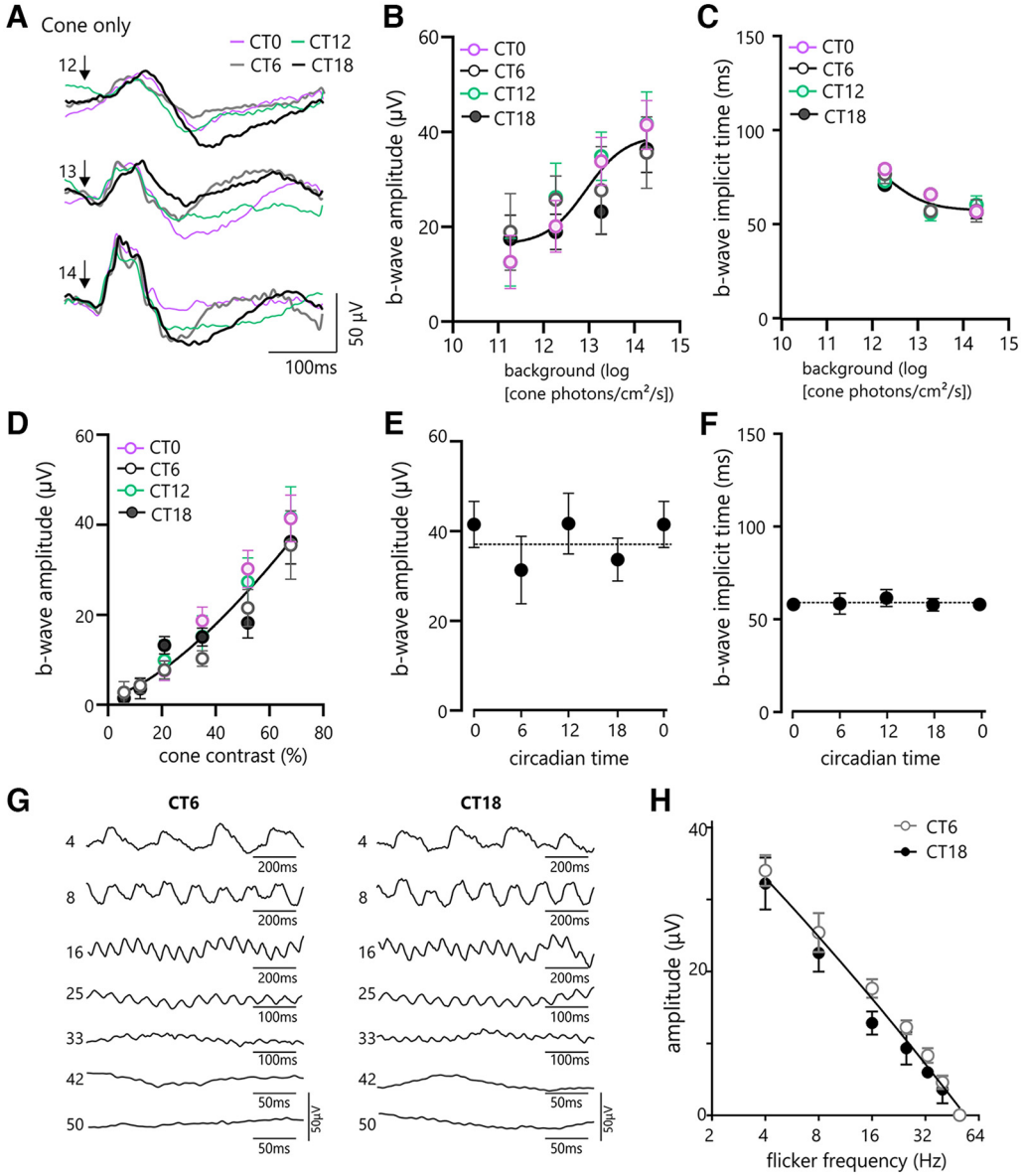

Figure 2. Circadian profile of mesopic cone vision. ***A***, Mean representative ERG traces at increasing mean light levels recorded at 12.3–14.3 log cone photons/cm^2/s. Arrow depicts timing of stimulus flash. ***B***, ***C***, b-Wave amplitudes (***B***) and implicit times (***C***) measured at a range of background irradiances (cone contrast, 68%) and at four CTs. A two-way ANOVA comparing b-wave amplitude as a function of CT and irradiance finds a significant effect of irradiance ($p < 0.01$) but not CT ($p = 0.88$). A two-way ANOVA comparing b-wave implicit time as a function of CT and irradiance finds a significant effect or irradiance ($p < 0.01$) but not CT ($p = 0.43$). ***D***, b-Wave amplitudes measured at a range of contrasts (mean irradiance, 10^{14} cone effective photons/cm^2/s), and at four CTs. Two-way ANOVA comparing b-wave amplitude as a function of CT and contrast finds significant effects of contrast ($p < 0.01$) but not CT ($p = 0.73$). ***E***, ***F***, Circadian profile of b-wave amplitude (contrast, 64%; mean irradiance, 14.3 cone effective photons/cm^2/s, ***E***) and implicit time (***F***). Data in ***E*** and ***F*** were fit with a straight line with slope at 0 and sine waves with wavelength at 24 h; an *F* test comparison of fits finds a straight line is the preferred model for all data shown ($p < 0.05$, $n = 6$). Data show mean ± SEM. ***G***, Representative ERG responses in response to cone-isolating stimuli presented as square wave flickers at frequencies of 4–50 Hz, measured at CT6 (gray) and CT18 (black). Left, Numbers indicate stimulus frequency in Hz. ***H***, Flicker response amplitude in response to cone stimuli presented at CT6 (gray) and CT18 (black) as a function of flicker frequency. Data are best fit with a single curve (*F* test, $p > 0.05$, $n = 6$). Data show mean ± SEM.

upper end of their sensitivity range (12.7 log rod photons/cm^2/s) immediately after a transition from dark-adapted to light-adapted conditions. Here, rod responses were measurable across the time course and remained broadly stable in amplitude. Unlike cone-isolating ERGs recorded in parallel (Fig. 3*L*,*M*), rod ERGs showed a maintained time-of-day difference after 20 min adaptation, peaking at CT18 (Fig. 4*G*,*H*).

Responses to square wave flickers of the rod stimulus were also recorded across a range of frequencies (4–50 Hz) at a background of 11.3 log rod photons/cm^2/s. A marked suppression in amplitude at CT6 versus CT18 (Fig. 4*I*,*J*) was again observed. However, normalizing for differences in amplitude revealed no change in temporal tuning itself but rather a change in amplitude across all stimulus frequencies (Fig. 4*K*).

Rhythms in light-adapted rod responses originate primarily in the secondary rod pathway

Consistent with previous work (Storch et al., 2007; Cameron et al., 2008a; Sengupta et al., 2011), the amplitude and implicit time of the scotopic ERG (recorded in dark-adapted conditions) were not significantly different at CT6 or CT18 (Fig. 5*A*–*C*). This confirms that the influence of the circadian clock is not intrinsic to

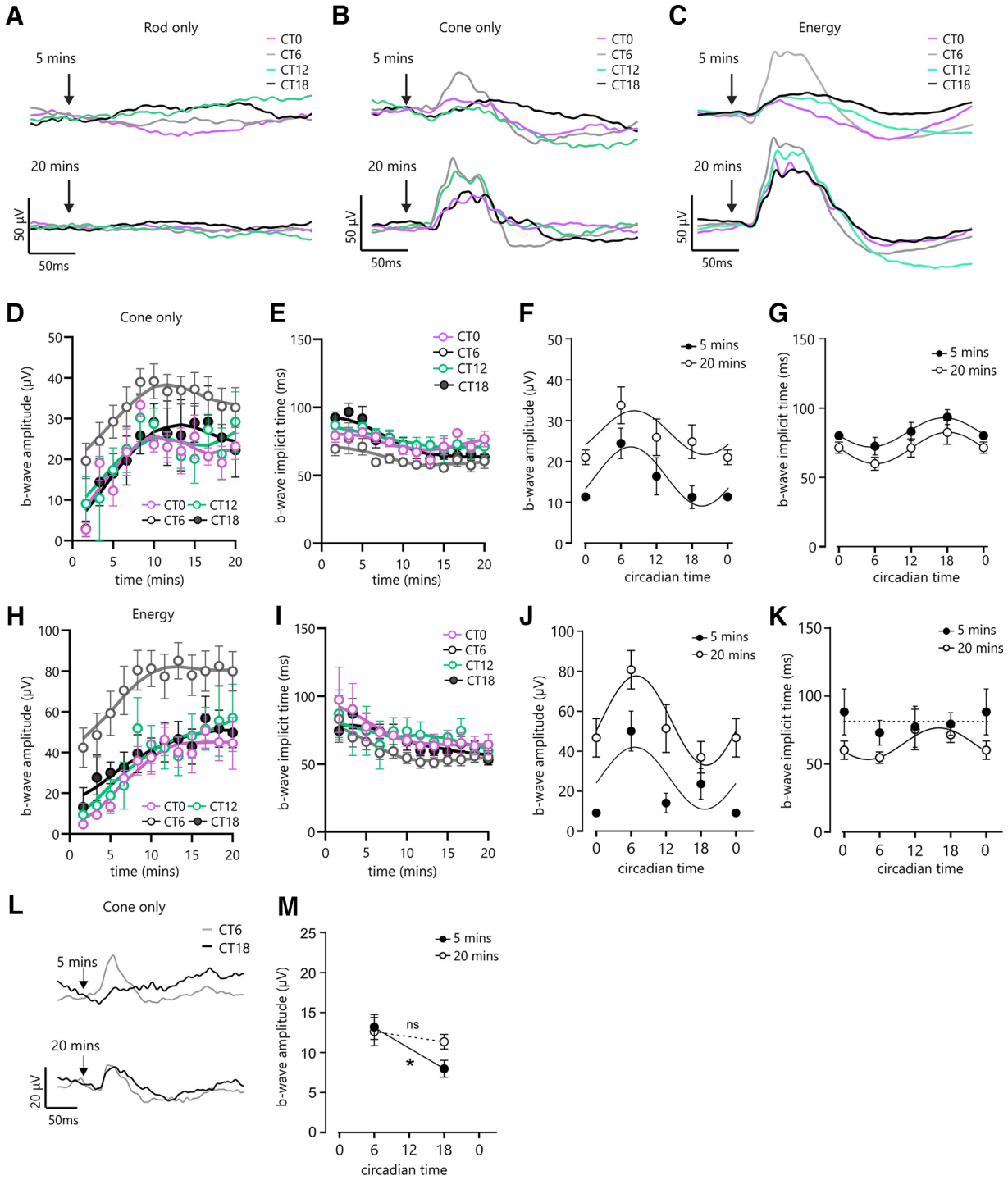

Figure 3. Dissecting photoreceptor contributions to the photopic ERG during light-adaptation. ***A–C***, Representative mean ERG traces after 5 min and 20 min of adaptation at CT0, 6, 12, and 18 in response to a rod-isolating (***A***), cone-isolating (***B***), or energy flash (***C***; background 15.3 log cone photons/cm^2/s; magenta, gray, cyan, and black lines represent CT0, 6, 12, and 18, respectively). ***D***, ***E***, b-Wave amplitude (***D***) and implicit time (***E***) in response to a cone-isolating flash, measured after different durations of light adaptation at four CTs. Two-way ANOVA comparing b-wave amplitude as a function of CT and adaptation time finds a significant effect of adaptation time and CT ($p < 0.01$). Two-way ANOVA comparing b-wave implicit time as a function of CT, and adaptation time finds a significant effect of adaptation time and CT ($p < 0.05$). ***F***, ***G***, Circadian profile of b-wave amplitude (***F***) and implicit time (***G***) in response to a cone-isolating flash after 5 min and 20 min of adaptation (filled and open circles, respectively). Data were fit with a straight line with slope at 0 and sine waves with wavelength at 24 h; an *F* test comparison of fits finds sine wave is the preferred model for all data shown ($p < 0.05$). ***H–I***, Same as ***D*** and ***E*** but for energy flashes. Two-way ANOVA comparing b-wave amplitude as a function of CT, and adaptation time finds a significant effect of adaptation time and CT ($p < 0.01$). Two-way ANOVA comparing b-wave implicit time as a function of CT, and adaptation time finds a significant effect of adaptation time and CT ($p < 0.05$). ***J–K***, Same as ***F*** and ***G*** but for energy flashes. Data were fit with a straight line with slope at 0 and sine waves with wavelength at 24 h; an *F* test comparison of fits finds sine wave is the preferred model for b-wave amplitude at 5 minutes and 20 minutes, and b-wave implicit time at 20 minutes ($p < 0.05$). ***L***, Representative mean ERG traces after 5 min and 20 min of adaptation at CT6 and CT18 in response to a cone-isolating flash (background 12.7 log cone photons/cm^2/s; gray and black lines represent CT6 and CT18, respectively). ***M***, b-Wave amplitude in response to a cone-isolating flash, measured after different durations of light adaptation at CT6 and CT18. Two-way ANOVA comparing b-wave amplitude as a function of CT, and adaptation time finds a significant effect of CT; *post hoc* Bonferroni comparing CT at each time point finds $p < 0.05$ for 5 min and $p > 0.05$ for 20 min adaptation; $n = 5–8$ per group. Data show mean ± SEM.

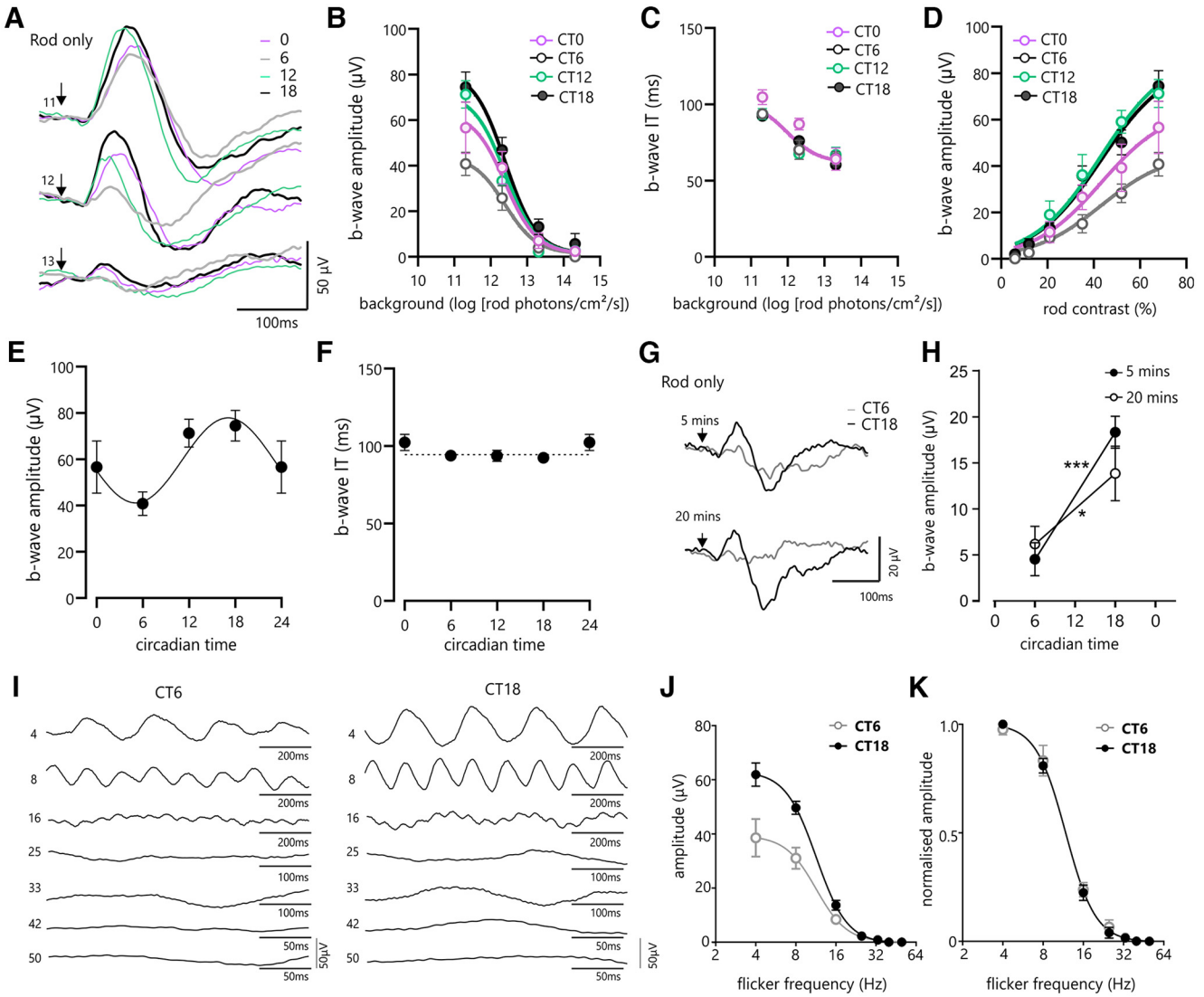

Figure 4. Circadian profile of mesopic rod responses. ***A***, Mean representative ERG traces at increasing mean light levels (log rod photons/cm^2/s, left of curves) at four CTs. Arrow depicts timing of stimulus flash. ***B***, ***C***, b-Wave amplitudes (***B***) and implicit times (***C***) measured at a range of background irradiances (rod contrast, 68%) and at four CTs. A two-way ANOVA comparing b-wave amplitude as a function of CT, and irradiance finds significant effects of CT and irradiance. *Post hoc* Bonferroni $p < 0.01$ for CT6 versus CT12 and CT6 versus CT18 at 11.3 log rod photons/cm^2/s; $p < 0.01$ for CT6 versus CT18 at 12.3 log rod photons/cm^2/s. ***D***, b-Wave amplitudes measured at a range of contrasts (mean irradiance, 11.3 log rod photons/cm^2/s) and at four CTs. Two-way ANOVA comparing b-wave amplitude as a function of CT and contrast; significant effects of CT and contrast. *Post hoc* Bonferroni $p < 0.01$ for CT6 versus CT12 and CT6 versus 18 at 68 and 52%; $p < 0.01$ for CT6 versus CT18 at 35%. ***E***, ***F***, Circadian profile of b-wave amplitude (contrast, 68%; mean irradiance, 10^{11} rod effective photons/cm^2/s, ***E***) and implicit time (***F***). Two-way ANOVA comparing b-wave implicit time as a function of CT and irradiance; significant effect of irradiance but not CT. Data in ***E*** and ***F*** were fit with a straight line with slope at 0 and sine waves with wavelength at 24 h; an *F* test comparison of fits finds a sigmoidal curve is the preferred model for b-wave amplitude ($p < 0.05$), and a straight line is the preferred model for implicit time ($p < 0.05$). ***G***, Representative mean ERG traces after 5 min and 20 min of adaptation at CT6 and CT18 in response to a rod-isolating flash (background 12.7 log cone photons/cm^2/s; gray and black lines represent CT6 and CT18, respectively). ***H***, b-Wave amplitude in response to a cone-isolating flash, measured after different durations of light adaptation at CT6 and CT18. Two-way ANOVA comparing b-wave amplitude as a function of CT, and adaptation time finds a significant effect of CT; *post hoc* Bonferroni comparing CT at each time point finds $p < 0.001$ for 5 min and $p < 0.05$ for 20 min adaptation. ***I***, Representative ERG responses in response to rod-isolating stimuli presented as square wave flickers at frequencies of 4–50 Hz, measured at CT6 (gray) and CT18 (black). Left, Numbers indicate stimulus frequency in Hz. ***J***, flicker response amplitude in response to rod stimuli presented at CT6 (gray) and CT18 (black) as a function of flicker frequency. Data are best fit with two separate curves (*F* test, $p < 0.05$). ***K***, Same data as ***J***, but data are normalized to maximum response. Data are best fit with a single curve (*F* test, $p > 0.05$; $n = 6$ for all data). Data show mean ± SEM.

rods themselves but rather in downstream elements of rod pathway(s). The fact that scotopic responses are arrhythmic also suggests that the circadian clock has a limited influence on the primary rod pathway, which conveys the highest sensitivity rod signals via rod bipolar cells, to Aii amacrine cells, to cone bipolar cells (Famiglietti and Kolb, 1975; Dacheux and Raviola, 1986; Strettoi et al., 1990).

Next, 2000 ms steps between spectra were used to separate ON and OFF aspects of the rod response. The amplitude of the b-wave (at light onset) and d-wave (at light offset, largely representing the activity of OFF bipolar cells; Stockton and Slaughter, 1989) were quantified at two time points (CT6 and CT18) at the extremes of this circadian rhythm. A time-of-day difference in amplitude analogous to that observed with a flash response was found for the b-wave (at light onset) but not d-wave (at light offset; Fig. 5*D–F*). This indicates that the circadian clock has a limited influence on the tertiary rod pathway (Soucy et al., 1998; Hack et al., 1999), which couples rods to OFF bipolar cells and so should respond preferentially to negative contrast stimuli.

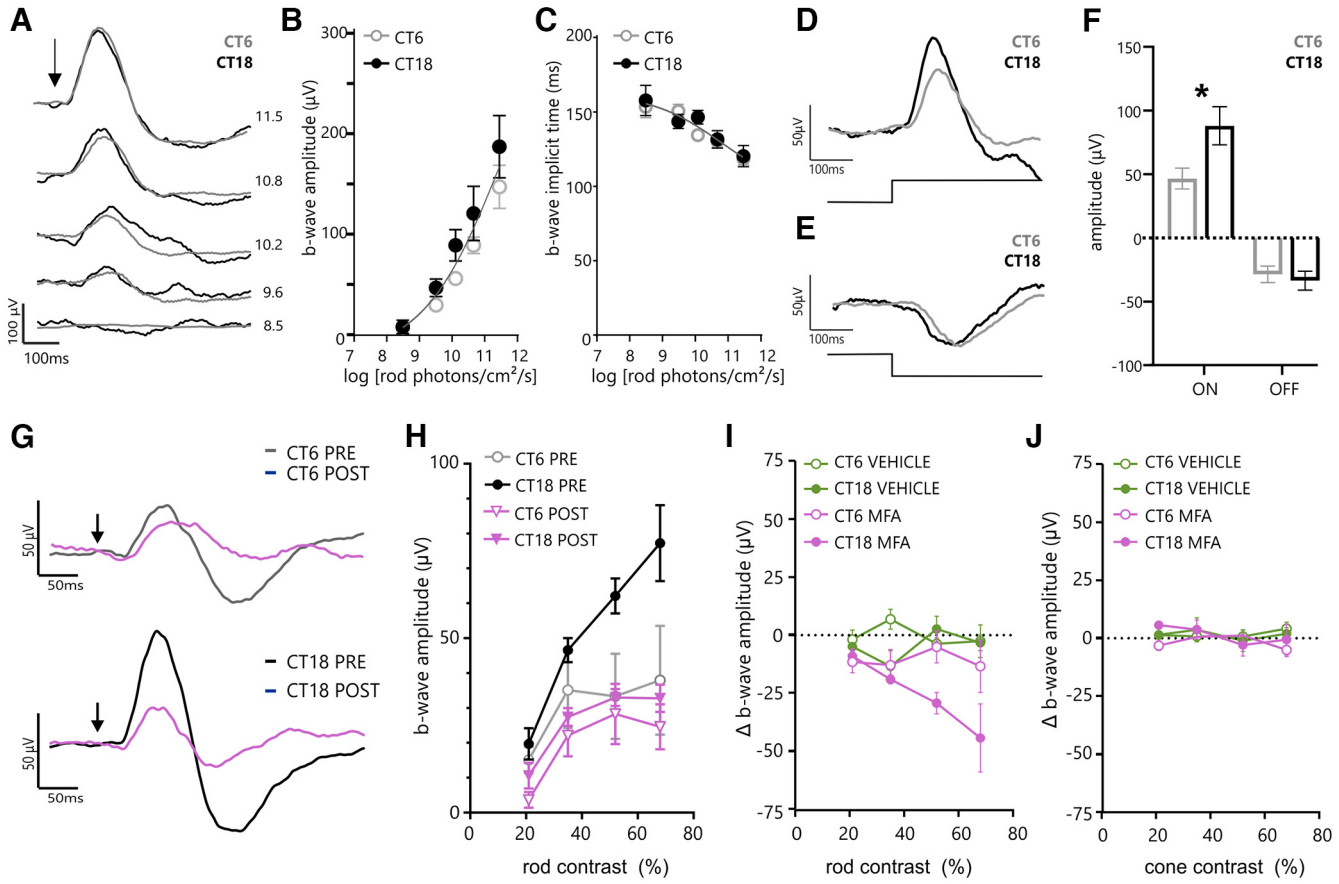

Figure 5. Establishing the conditions in which rod visual responses are rhythmic. ***A***, Representative ERG traces in response to flashes presented against darkness measured at CT6 (gray) and CT18 (black); intensity in log rod photons/cm^2/s; right of curves. ***B***, ***C***, b-Wave amplitude (***B***) and implicit time (***C***) as a function of stimulus intensity. A two-way ANOVA comparing b-wave amplitude as a function of CT and irradiance finds a significant effect of irradiance ($p < 0.001$) but not CT ($p = 0.23$) or an interaction ($p = 0.37$). A two-way ANOVA comparing b-wave implicit time as a function of CT and irradiance; significant effect of irradiance ($p < 0.001$) but not CT ($p = 0.71$) or an interaction ($p = 0.28$). ***D***, ***E***, Representative ERG traces in response to positive (***D***) and negative (***E***) rod contrast steps recorded at CT6 and CT18 (gray and black, respectively). Bottom, Lines depict timing of the change in stimulus. ***F***, Bar graph showing mean ± SEM response amplitudes to positive (ON) and negative (OFF) rod contrast steps, recorded at CT6 and CT18 (gray and black, respectively) at a background of 10^{12} log photons/cm^2/s. Two-way ANOVA comparing ON and OFF response amplitude as a function of CT; significant effects of CT. *Post hoc* Bonferroni $p < 0.05$ for CT6 versus CT18 ON response but not OFF ($p = 0.41$). ***G***, ERG waveforms recorded before (black and gray) and after intravitreal injection of 1 mM MFA (magenta) at CT6 and CT18. ***H***, ERG response amplitude as a function of rod contrast, shown before and after intravitreal injection of 1 mM MFA at CT6 versus CT18 (gray open and black closed circles represent CT6 and CT18 before injection, respectively; magenta open and closed triangles represent CT6 and CT18 after 1 mM MFA injection, respectively). Two-way ANOVAs compared data before and after intravitreal injection of MFA at CT6 and CT18 and found significant effects of the drug at CT18 ($p < 0.005$) but not CT6 ($p = 0.11$). ***I***, The difference in b-wave amplitude following intravitreal injection of 1 mM MFA or vehicle at CT6 and CT18 across a range of rod contrasts presented at a background of 10^{12} log photons/cm^2/s (green open and closed circles represent CT6 and CT18 after vehicle injection, respectively; magenta open and closed triangles represent CT6 and CT18 after 1 mM MFA injection, respectively). ***J***, Difference in b-wave amplitude following intravitreal injection of 1 mM MFA or vehicle at CT6 and CT18 across a range of cone contrasts (green open and closed circles represent CT6 and CT18 after vehicle injection, respectively; magenta open and closed triangles represent CT6 and CT18 after 1 mM MFA injection, respectively). Stimuli presented at 10^{12} log photons/cm^2/s; $N = 5$ for each group. Data show mean ± SEM.

The remaining route of rod signals through the retina originates with gap junction coupling between rods and cones – the secondary rod pathway (Nelson, 1977; Schneeweis and Schnapf, 1995). There is evidence that this coupling is under circadian control (at least in melatonin sufficient strains (Ribelayga et al., 2008). To test whether the strength of this coupling was the origin of rhythms in mesopic rod responses, ERGs were recorded before and after an intravitreal injection of the gap junction blocker MFA (2 µl of 1 mM MFA). Light-adapted rod and cone ERGs were measured at CT6 versus CT18 at a background intensity where both rod and cone responses were measurable (10^{12} rod effective photons/cm^2/s). MFA produced a reduction in rod b-wave amplitude at both time points, but this was much more substantial at CT18 (Fig. 5*G–I*). The upshot was that MFA treatment removed the significant circadian variation in rod response amplitude. No such impact was observed following vehicle injection. By comparison, cone ERGs, recorded in parallel, show no significant impact of MFA injection at either circadian time point (Fig. 5*J*). This indicates that a change in rod-to-cone coupling has a pronounced impact on rod signals appearing in cone pathways, but the same is not necessarily true for cone signals appearing in rod pathways (presumably because of response saturation in the primary rod pathway).

Rhythms in rod response amplitude are relayed through the primary visual pathway

To establish whether rhythms in response amplitude were propagated beyond the retina, responses were recorded in the dLGN of anesthetized *Opn1mw^R* mice. Using multichannel recording electrodes, light-evoked changes in firing were recorded in response to rod- and cone-isolating stimuli. Rod responses were only measurable at the lower light level, which is consistent with the range over which rod ERGs were measurable (Fig. 6*A*, *B*). Also in agreement with ERG data, rod response amplitudes

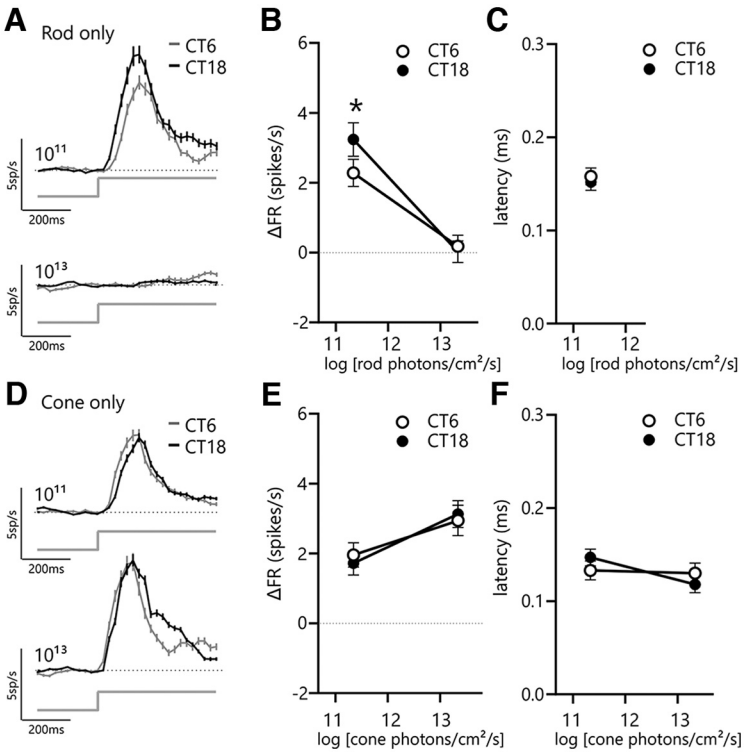

Figure 6. Time of day variation in the amplitude of rod but not cone responses in the dLGN. ***A***, Mean ± SEM firing rate at the onset of a 2 s rod step presented at two mean light levels (11.3 and 13.3 log photons/cm^2/s), recorded at CT6 and CT18 (gray and black lines, respectively; data show mean ± SEM). ***B***, Change in firing rate in the first 250 ms of a rod-isolating stimulus. Mixed-effects linear model with *post hoc* Sidak correction finds $p < 0.01$ for CT6 versus CT18 at 11.3 log photons/cm^2/s. ***C***, Response latency (time to maximum response) following onset of a rod-isolating stimulus. A mixed-effects linear model finds no significant effect of CT. ***D–F***, Same as ***A–C*** but using cone-isolating stimuli. A mixed-effects linear model with *post hoc* Sidak correction finds $p > 0.05$ for CT6 versus CT18 for amplitude and latency. Data show mean ± SEM ($n = 5$ animals at each time point, $n = 186$ light-responsive units for CT6, $n = 217$ light-responsive units for CT18).

in the dLGN were significantly larger for recordings made at CT18 compared with CT6. Response latency (time-to-peak firing) was equivalent at each time point (Fig. 6*C*). These data indicate that rhythms in retinal rod responses are inherited by the early visual system and result in a change in light-evoked firing according to time of day. In contrast, cone-isolating stimuli drove robust changes in firing at each background irradiance level. In agreement with ERG responses, these responses were equivalent in amplitude and latency when measured at CT6 or CT18 (Fig. 6*D–F*).

Contrast–response functions are stable across the mesopic range in the circadian day but not night

In natural viewing, changes in radiance will typically be apparent for both photoreceptors in parallel. To therefore understand how independent rhythms that are apparent in rods versus cones combine when both are active, stimuli that excited both photoreceptors concurrently (rod-plus-cone) were applied (Michelson contrast matched to individual rod-isolating and cone-isolating stimuli). ERG responses were recorded in response to rod-plus-cone stimuli at a range of mean light intensities and contrasts, at CT6 and CT18. ERG responses were measurable across the full breadth of light intensities covered (Fig. 7*A–C*). At CT6 response amplitudes were stable throughout the mesopic to photopic range, and contrast–response functions remained constant across the range of background intensities tested (i.e., covering the transition between rod and cone dominated vision; Fig. 7*B*,*E*). In contrast, at CT18 as light intensity increased there was an initial decline in response amplitude, after which response amplitude stabilized (Fig. 7*A*,*B*). This was also evident in contrast–response functions in which the amplitude at dimmer backgrounds was enhanced compared with brighter backgrounds (Fig. 7*F*). The b-wave implicit time, on the other hand, showed a similar relationship at CT6 and CT18, whereby a gradual reduction in amplitude occurred as background irradiance increased (Fig. 7*C*,*G*,*H*).

This relationship was also explored in the dLGN, where the neural response to stimuli presenting contrast to rods and cones concurrently was compared at CT6 and CT18 (Fig. 7*I–K*). Consistent with retinal data, response amplitudes were significantly larger at CT18 versus CT6 when stimuli were presented against a mesopic backgrounds (Fig. 7*J*). In contrast, at low-photopic intensities, there was no longer any significant effect of circadian time. These data also support the conclusion that there is greater stability in response amplitude across the transition from rod- to cone-based vision in the circadian day compared with the night, where response amplitude is enhanced at lower mean light levels.

Discussion

By exploring vision at the extremes of sensitivity, past work has shown that the circadian clock is a critical regulator of photopic (cone only) but not scotopic (rod only) vision. However, vision frequently occurs between these two extremes, where both rods and cones are active and can contribute to vision. In this study, the method of receptor silent substitution has been used to characterize the influence of the circadian clock on rod versus cone responses throughout this mesopic range. This revealed that cone vision is arrhythmic in mesopic to photopic conditions, with the daytime peak in amplitude and implicit time only emerging following a sharp transition from darkness to bright light. On the other hand, there is a pronounced rhythm in mesopic rod vision so that rod ERG responses are almost double in amplitude in the subjective night compared with the subjective day. These effects are relayed to the dLGN, where rhythms are detectable in rod, but not cone, response amplitude in mesopic conditions. The upshot is that combined rod-plus-cone responses have a stable contrast–response relationship across light levels in the circadian day but are enhanced at low light at night. Ultimately, these data support the view that the circadian clock is a key regulator of vision specifically in regulating the balance of rod versus cone visual responses at mesopic light levels according to time of day.

A marked rhythm in rod vision is apparent in mesopic conditions with an almost two-fold change in ERG b-wave amplitude occurring between subjective midday and midnight. This finding was consistent with a change in overall gain in rod responses as no obvious shift in contrast–response functions or temporal tuning curves was found between time points when normalized to the maximum response. The fact that rod vision is rhythmic in these conditions is perhaps surprising, given that the majority of previous work has not identified rhythmicity in ERGs recorded

in the rod range (but see Gegnaw et al., 2021). However, because rod responses traverse the retina via three known routes (Bloomfield and Dacheux, 2001; Bloomfield and Volgyi, 2009; Grimes et al., 2018), a straightforward explanation is that the rhythms observed here originate with the secondary rod pathway, which dominates rod vision in mesopic conditions (DeVries and Baylor, 1995), and in which rods and cones are coupled directly via gap junctions (Nelson, 1977; Schneeweis and Schnapf, 1999; Deans et al., 2002; Abd-El-Barr et al., 2009). Consistent with that view, the circadian variation in light-adapted rod responses is removed by the gap-junction blocker MFA, indicating that circadian rhythms in photoreceptor gap-junction coupling are a likely origin of rhythms in rod response amplitude (Ribelayga et al., 2008).

The strength of rod-cone coupling in the mouse retina is under the control of dopamine and adenosine (Li et al., 2013). Circadian rhythms in retinal dopamine are driven by melatonin, and it has been inferred that melatonin is necessary to drive rhythms in photoreceptor coupling (Ribelayga et al., 2008). However, most strains of lab mice do not produce melatonin, and evidence of a functional rhythm in coupling in melatonin-deficient backgrounds, such as C57/BL6 used here, is absent. Nevertheless, Cx36 transcript expression does remain rhythmic in these strains, peaking in the night (Katti et al., 2013). In addition, although dopamine circadian rhythms are driven by melatonin, rhythms in dopamine receptor expression do not require melatonin (Jackson et al., 2011) and could arguably support rhythmic changes in coupling.

Robust rhythms in cone vision are revealed when moving from dark-adapted to very bright (photopic) conditions and peak in the subjective day, in antiphase to rods. However, here we have found that no rhythmicity is apparent in cone responses across their sensitivity range following a period of adaptation. A simple interpretation of this result is that it represents a rhythm in the efficiency of light adaptation, and this is consistent with the fact that cone visual responses are arrhythmic when measured after long-term light exposure (Barnard et al., 2006) and following the loss of dopaminergic signaling (Jackson et al., 2012). Previous work has also highlighted a role for melanopsin in driving cone ERG rhythms (Barnard et al., 2006), and because melanopsin is a driver of light adaptation (Allen et al., 2014; Milosavljevic et al., 2016), it is possible that rhythms in the photopic ERG represent a rhythms in ipRGC-driven adaptation.

Both environmental and behavioral factors (e.g., changing cloud cover, an animal entering a burrow) mean that daytime light intensities can cover the full visual range. Here, we have observed that contrast–response functions of the combined rod-plus-cone output is stable across much of this range in the circadian day. Therefore, a relative dampening of rod-driven responses in the day can ensure that the response to contrast is stable in the transition between rod- and cone-dominated vision (at least for full field stimuli at this stimulus frequency). These data are consistent with a behavioral assay of contrast sensitivity in mice (conducted in the subjective day), which demonstrates Weber-like adaptation across the mesopic range at low temporal frequencies (Umino et al., 2018). This stable

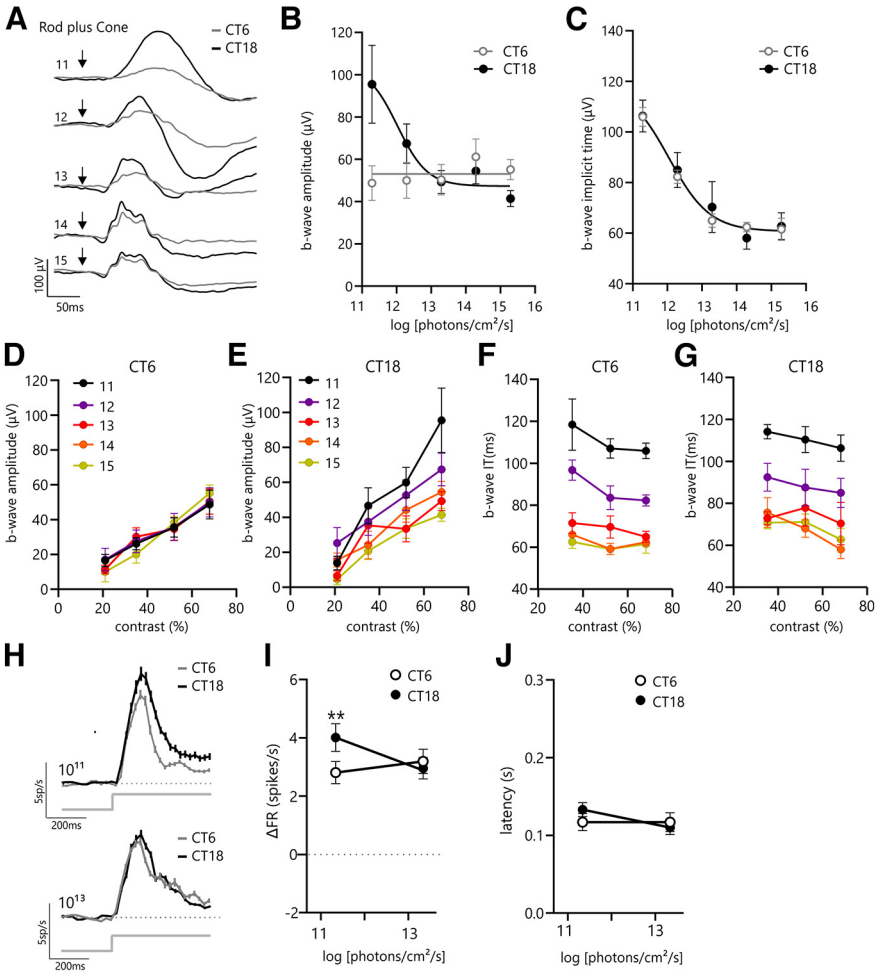

Figure 7. Circadian profile of rod-plus-cone responses measured across the mesopic–photopic transition. ***A***, Mean representative ERG traces at increasing mean light levels (log photons/cm^2/s, left of curves), measured at CT6 (pink) and CT18 (gray). Arrow depicts timing of stimulus flash. ***B***, ***C***, b-Wave amplitude (***B***) and implicit time (***C***) in response to a rod-plus-cone stimulus (68% Michelson contrast) measured at a range of background irradiances at CT6 and CT18. A two-way ANOVA comparing b-wave amplitude as a function of CT and irradiance finds a significant effect of irradiance ($p < 0.05$) but not CT ($p = 0.11$) with a significant interaction ($p < 0.01$). ***D–G***, b-Wave amplitudes (***D–E***) and implicit times (***F–G***) to stimuli of increasing contrasts, recorded at a range of mean background irradiances at CT6 (***D***, ***F***) and CT18 (***E***, ***G***). At CT6, a two-way ANOVA comparing b-wave amplitude as a function of irradiance and contrast finds a significant effect of contrast ($p < 0.001$) but not irradiance ($p = 0.99$) with no interaction. A two-way ANOVA comparing b-wave implicit time finds a significant effect of contrast ($p < 0.01$) and irradiance ($p < 0.001$). At CT18, a two-way ANOVA comparing b-wave amplitude as a function of irradiance and contrast finds a significant effect of contrast ($p < 0.001$) and irradiance ($p < 0.05$), with a significant interaction ($p < 0.01$). A two-way ANOVA comparing b-wave IT finds a significant effect of contrast ($p < 0.05$) and irradiance ($p < 0.01$). ***H***, Mean ± SEM change in firing rate at the onset of a 2 s rod-plus-cone step presented at two mean light levels (11.3 and 13.3 log photons/cm^2/s), recorded at CT6 and CT18 (gray and black lines, respectively). Data show mean ± SEM. ***I***, Change in firing rate in the first 250 ms of a rod-plus-cone stimulus. A mixed-effects linear model with *post hoc* Sidak correction finds $p < 0.01$ for CT6 versus CT18 at 11.3 log photons/cm^2/s but not 13.3 log photons/cm^2/s. ***J***, Response latency (time to maximum response) following onset of a rod-plus-cone stimulus. A mixed-effects linear model finds no significant effect of CT. Data show mean ± SEM ($n = 5$ animals at each time point, $n = 186$ light-responsive units for CT6, $n = 217$ light-responsive units for CT18).

response does not occur in the subjective night; rod (and therefore combined rod-plus-cone) responses are anomalously large at lower mean light levels, meaning there is a relative difference in amplitude to a fixed contrast across the transition from rod to cone vision. At night, however, there is no natural advantage in preserving irradiance-invariant contrast responses above the rod range as light intensities never would naturally exceed this.

The circadian clock drives changes in the retinal network that favor rod vision at night, but the advent of artificial lighting means that nighttime light intensities can regularly move out of the (exclusively) rod range. Contrast–response amplitudes are not conserved across the rod-cone transition at night, which would imply that visual responses would be much less consistent when moving across the mesopic-photopic range, and could reasonably affect visual performance in such conditions. This notion extends across the animal kingdom, where there are examples of amplified rod-based vision at night and/or amplified cone-based vision in the day in birds, fish, and amphibia (Wang and Mangel, 1996; Krizaj et al., 1998; Li and Dowling, 1998; Manglapus et al., 1999; Ribelayga et al., 2008). At the very extreme are larval zebrafish, which entirely shut down cone vision at night by disassembling cone synaptic pedicles (Li and Dowling, 1998). Artificially lit night environments may therefore present a sensory challenge to numerous species, and further work is required to establish what short- and/or long-term consequences there might be on the function and overall health of the retina.

Here, the daytime rod ERG became undetectable at $\sim 10^{13}$ photons/cm^2/s ($\sim 10^4$ R*/rod/s), defining the upper limit of mesopic vision in this experimental paradigm. Although care must be taken in making direct comparisons between different physiological and behavioral measures of rod saturation and when using knock-out mice (where remaining visual pathways may not be functioning entirely normally), this value is comparable to that reported in cone-deficient mice for maze navigation (Nathan et al., 2006), ERG responses (Tanimoto et al., 2015), psychophysical assessments (Naarendorp et al., 2010), and circadian photoentrainment (Altimus et al., 2008). In addition, however, it is important to note that rods recover from saturation in light-adapted conditions so that after prolonged light exposure, rod responses can occur at intensities that extend well into the classical photopic range (Tikidji-Hamburyan et al., 2017; Frederiksen et al., 2021). These studies highlight the important point that rod saturation is not an absolute value; it very much depends on factors such as the experimental conditions (especially adaptational state of rods), as well as species studies, and end point measured.

Although mesopic rod and rod-plus-cone responses showed significant changes in amplitude between CT6 and CT18, ERG implicit times and dLGN response latencies were remarkably stable between conditions. Most intriguingly, those data imply that separate neural mechanisms govern the amplitude and latency of rod/cone responses in these conditions. This separation could be a valuable way to better understand the involvement of circadian processes in regulating individual components of rod/cone circuits. Similarly, although the implicit times of rod-only or cone-only ERG responses both decreased as background light intensity rose, rod and cone ERGs showed comparable kinetics for any given background (Fig. 1*F*). Temporal differences between rods and cones can have profound effects on vision (Stockman and Sharpe, 2006), and so synchronizing response kinetics in this way will be important in reducing signal interference between these two systems.

In conclusion, this work has established that rod- and cone-driven visual responses are differentially regulated by the circadian clock in the mesopic-photopic transition. These rhythms effectively stabilize contrast–response amplitude in the circadian day and boost rod responses at low light at night. This change in amplitude is also apparent in the early visual system (dLGN) in response to full-field contrast steps visible to rods/rods and cones. However, simple light responses are transformed by the early visual system into multiple parallel outputs, which encode visual features other than full-field changes in light intensity. There is evidence that the circadian clock influences certain subsets of retinal ganglion cells to modulate aspects of spatial contrast sensitivity (Hwang et al., 2013), which in turn can regulate visual behavior (Hwang et al., 2013; Wong et al., 2018). An obvious area of future work, therefore, will be to establish how the clock ultimately regulates vision across the full breadth of the visual code.

References

Abd-El-Barr MM, Pennesi ME, Saszik SM, Barrow AJ, Lem J, Bramblett DE, Paul DL, Frishman LJ, Wu SM (2009) Genetic dissection of rod and cone pathways in the dark-adapted mouse retina. J Neurophysiol 102:1945–1955.

Ait-Hmyed Hakkari O, Acar N, Savier E, Spinnhirny P, Bennis M, Felder-Schmittbuhl MP, Mendoza J, Hicks D (2016) Rev-Erbα modulates retinal visual processing and behavioral responses to light. FASEB J 30:3690–3701.

Allen AE, Lucas RJ (2016) Using silent substitution to track the mesopic transition from rod- to cone-based vision in mice. Invest Ophthalmol Vis Sci 57:276–287.

Allen AE, Storchi R, Martial FP, Petersen RS, Montemurro MA, Brown TM, Lucas RJ (2014) Melanopsin-driven light adaptation in mouse vision. Curr Biol 24:2481–2490.

Altimus CM, Guler AD, Villa KL, McNeill DS, Legates TA, Hattar S (2008) Rods-cones and melanopsin detect light and dark to modulate sleep independent of image formation. Proc Natl Acad Sci U S A 105:19998–20003.

Barnard AR, Hattar S, Hankins MW, Lucas RJ (2006) Melanopsin regulates visual processing in the mouse retina. Curr Biol 16:389–395.

Bloomfield SA, Dacheux RF (2001) Rod vision: pathways and processing in the mammalian retina. Prog Retin Eye Res 20:351–384.

Bloomfield SA, Volgyi B (2009) The diverse functional roles and regulation of neuronal gap junctions in the retina. Nat Rev Neurosci 10:495–506.

Brown TM, Tsujimura S, Allen AE, Wynne J, Bedford R, Vickery G, Vugler A, Lucas RJ (2012) Melanopsin-based brightness discrimination in mice and humans. Curr Biol 22:1134–1141.

Cameron MA, Lucas RJ (2009) Influence of the rod photoresponse on light adaptation and circadian rhythmicity in the cone ERG. Mol Vis 15:2209–2216.

Cameron MA, Barnard AR, Hut RA, Bonnefont X, van der Horst GT, Hankins MW, Lucas RJ (2008a) Electroretinography of wild-type and Cry mutant mice reveals circadian tuning of photopic and mesopic retinal responses. J Biol Rhythms 23:489–501.

Cameron MA, Barnard AR, Lucas RJ (2008b) The electroretinogram as a method for studying circadian rhythms in the mammalian retina. J Genet 87:459–466.

Dacheux RF, Raviola E (1986) The rod pathway in the rabbit retina: a depolarizing bipolar and amacrine cell. J Neurosci 6:331–345.

Deans MR, Volgyi B, Goodenough DA, Bloomfield SA, Paul DL (2002) Connexin36 is essential for transmission of rod-mediated visual signals in the mammalian retina. Neuron 36:703–712.

DeVries SH, Baylor DA (1995) An alternative pathway for signal flow from rod photoreceptors to ganglion cells in mammalian retina. Proc Natl Acad Sci U S A 92:10658–10662.

Doyle SE, Grace MS, McIvor W, Menaker M (2002) Circadian rhythms of dopamine in mouse retina: the role of melatonin. Vis Neurosci 19:593–601.

Estevez O, Spekreijse H (1982) The "silent substitution" method in visual research. Vision Res 22:681–691.

Famiglietti EV Jr, Kolb H (1975) A bistratified amacrine cell and synaptic circuitry in the inner plexiform layer of the retina. Brain Res 84:293–300.
Frederiksen R, Morshedian A, Tripathy SA, Xu T, Travis GH, Fain GL, Sampath AP (2021) Rod photoreceptors avoid saturation in bright light by the movement of the G protein transducin. J Neurosci 41:3320–3330.
Fukuhara C, Liu C, Ivanova TN, Chan GC, Storm DR, Iuvone PM, Tosini G (2004) Gating of the cAMP signaling cascade and melatonin synthesis by the circadian clock in mammalian retina. J Neurosci 24:1803–1811.
Gegnaw ST, Sandu C, Mendoza J, Bergen AA, Felder-Schmittbuhl MP (2021) Dark-adapted light response in mice is regulated by a circadian clock located in rod photoreceptors. Exp Eye Res 213:108807.
Govardovskii VI, Fyhrquist N, Reuter T, Kuzmin DG, Donner K (2000) In search of the visual pigment template. Vis Neurosci 17:509–528.
Grimes WN, Songco-Aguas A, Rieke F (2018) Parallel processing of rod and cone signals: retinal function and human perception. Annu Rev Vis Sci 4:123–141.
Hack I, Peichl L, Brandstatter JH (1999) An alternative pathway for rod signals in the rodent retina: rod photoreceptors, cone bipolar cells, and the localization of glutamate receptors. Proc Natl Acad Sci U S A 96:14130–14135.
Hwang CK, Chaurasia SS, Jackson CR, Chan GC, Storm DR, Iuvone PM (2013) Circadian rhythm of contrast sensitivity is regulated by a dopamine-neuronal PAS-domain protein 2-adenylyl cyclase 1 signaling pathway in retinal ganglion cells. J Neurosci 33:14989–14997.
Jackson CR, Chaurasia SS, Hwang CK, Iuvone PM (2011) Dopamine D(4) receptor activation controls circadian timing of the adenylyl cyclase 1/cyclic AMP signaling system in mouse retina. Eur J Neurosci 34:57–64.
Jackson CR, Ruan GX, Aseem F, Abey J, Gamble K, Stanwood G, Palmiter RD, Iuvone PM, McMahon DG (2012) Retinal dopamine mediates multiple dimensions of light-adapted vision. J Neurosci 32:9359–9368.
Jacobs GH, Williams GA (2007) Contributions of the mouse UV photopigment to the ERG and to vision. Doc Ophthalmol 115:137–144.
Katti C, Butler R, Sekaran S (2013) Diurnal and circadian regulation of connexin 36 transcript and protein in the mammalian retina. Invest Ophthalmol Vis Sci 54:821–829.
Koskela S, Turunen T, Ala-Laurila P (2020) Mice reach higher visual sensitivity at night by using a more efficient behavioral strategy. Curr Biol 30:42–53.e4.
Krizaj D, Gabriel R, Owen WG, Witkovsky P (1998) Dopamine D2 receptor-mediated modulation of rod-cone coupling in the *Xenopus* retina. J Comp Neurol 398:529–538.
LaVail MM (1976) Rod outer segment disk shedding in rat retina: relationship to cyclic lighting. Science 194:1071–1074.
Li H, Zhang Z, Blackburn MR, Wang SW, Ribelayga CP, O'Brien J (2013) Adenosine and dopamine receptors coregulate photoreceptor coupling via gap junction phosphorylation in mouse retina. J Neurosci 33:3135–3150.
Li L, Dowling JE (1998) Zebrafish visual sensitivity is regulated by a circadian clock. Vis Neurosci 15:851–857.
Lucas RJ, Lall GS, Allen AE, Brown TM (2012) How rod, cone, and melanopsin photoreceptors come together to enlighten the mammalian circadian clock. Prog Brain Res 199:1–18.
Manglapus MK, Iuvone PM, Underwood H, Pierce ME, Barlow RB (1999) Dopamine mediates circadian rhythms of rod-cone dominance in the Japanese quail retina. J Neurosci 19:4132–4141.
Milosavljevic N, Allen AE, Cehajic-Kapetanovic J, Lucas RJ (2016) Chemogenetic activation of ipRGCs drives changes in dark-adapted (scotopic) electroretinogram. Invest Ophthalmol Vis Sci 57:6305–6312.
Naarendorp F, Esdaille TM, Banden SM, Andrews-Labenski J, Gross OP, Pugh EN Jr (2010) Dark light, rod saturation, and the absolute and incremental sensitivity of mouse cone vision. J Neurosci 30:12495–12507.
Nathan J, Reh R, Ankoudinova I, Ankoudinova G, Chang B, Heckenlively J, Hurley JB (2006) Scotopic and photopic visual thresholds and spatial and temporal discrimination evaluated by behavior of mice in a water maze. Photochem Photobiol 82:1489–1494.
Nelson R (1977) Cat cones have rod input: a comparison of the response properties of cones and horizontal cell bodies in the retina of the cat. J Comp Neurol 172:109–135.
Peachey NS, Ball SL (2003) Electrophysiological analysis of visual function in mutant mice. Doc Ophthalmol 107:13–36.
Ribelayga C, Mangel SC (2005) A circadian clock and light/dark adaptation differentially regulate adenosine in the mammalian retina. J Neurosci 25:215–222.
Ribelayga C, Cao Y, Mangel SC (2008) The circadian clock in the retina controls rod-cone coupling. Neuron 59:790–801.
Rushton WA (1972) Pigments and signals in colour vision. J Physiol 220:1P–31P.
Schneeweis DM, Schnapf JL (1995) Photovoltage of rods and cones in the macaque retina. Science 268:1053–1056.
Schneeweis DM, Schnapf JL (1999) The photovoltage of macaque cone photoreceptors: adaptation, noise, and kinetics. J Neurosci 19:1203–1216.
Sengupta A, Baba K, Mazzoni F, Pozdeyev NV, Strettoi E, Iuvone PM, Tosini G (2011) Localization of melatonin receptor 1 in mouse retina and its role in the circadian regulation of the electroretinogram and dopamine levels. PLoS One 6:e24483.
Smallwood PM, Olveczky BP, Williams GL, Jacobs GH, Reese BE, Meister M, Nathans J (2003) Genetically engineered mice with an additional class of cone photoreceptors: implications for the evolution of color vision. Proc Natl Acad Sci U S A 100:11706–11711.
Soucy E, Wang Y, Nirenberg S, Nathans J, Meister M (1998) A novel signaling pathway from rod photoreceptors to ganglion cells in mammalian retina. Neuron 21:481–493.
Stockman A, Sharpe LT (2006) Into the twilight zone: the complexities of mesopic vision and luminous efficiency. Ophthalmic Physiol Opt 26:225–239.
Stockton RA, Slaughter MM (1989) B-wave of the electroretinogram. A reflection of ON bipolar cell activity. J Gen Physiol 93:101–122.
Storch KF, Paz C, Signorovitch J, Raviola E, Pawlyk B, Li T, Weitz CJ (2007) Intrinsic circadian clock of the mammalian retina: importance for retinal processing of visual information. Cell 130:730–741.
Strettoi E, Dacheux RF, Raviola E (1990) Synaptic connections of rod bipolar cells in the inner plexiform layer of the rabbit retina. J Comp Neurol 295:449–466.
Tanimoto N, Sothilingam V, Kondo M, Biel M, Humphries P, Seeliger MW (2015) Electroretinographic assessment of rod- and cone-mediated bipolar cell pathways using flicker stimuli in mice. Sci Rep 5:10731.
Tikidji-Hamburyan A, Reinhard K, Storchi R, Dietter J, Seitter H, Davis KE, Idrees S, Mutter M, Walmsley L, Bedford RA, Ueffing M, Ala-Laurila P, Brown TM, Lucas RJ, Münch TA (2017) Rods progressively escape saturation to drive visual responses in daylight conditions. Nat Commun 8:1813.
Tosini G, Menaker M (1996) Circadian rhythms in cultured mammalian retina. Science 272:419–421.
Tsai TI, Joachimsthaler A, Kremers J (2017) Mesopic and photopic rod and cone photoreceptor-driven visual processes in mice with long-wavelength-shifted cone pigments. Invest Ophthalmol Vis Sci 58:5177–5187.
Umino Y, Solessio E, Barlow RB (2008) Speed, spatial, and temporal tuning of rod and cone vision in mouse. J Neurosci 28:189–198.
Umino Y, Pasquale R, Solessio E (2018) Visual temporal contrast sensitivity in the behaving mouse shares fundamental properties with human psychophysics. eNeuro 5:ENEURO.0181-18.2018.
Umino Y, Guo Y, Chen CK, Pasquale R, Solessio E (2019) Rod photoresponse kinetics limit temporal contrast sensitivity in mesopic vision. J Neurosci 39:3041–3056.
Wang Y, Mangel SC (1996) A circadian clock regulates rod and cone input to fish retinal cone horizontal cells. Proc Natl Acad Sci U S A 93:4655–4660.
Wong JCY, Smyllie NJ, Banks GT, Pothecary CA, Barnard AR, Maywood ES, Jagannath A, Hughes S, van der Horst GTJ, MacLaren RE, Hankins MW, Hastings MH, Nolan PM, Foster RG, Peirson SN (2018) Differential roles for cryptochromes in the mammalian retinal clock. FASEB J 32:4302–4314.